JOURNAL OF GEOPHYSICAL RESEARCH, VOL. 113, G03S04, doi:10.1029/2007JG000559, 2008

Differential frost heave model for patterned ground formation: Corroboration with observations along a North American arctic transect

R. A. Peterson[1] and W. B. Krantz[2]

Received 24 July 2007; revised 7 November 2007; accepted 31 December 2007; published 2 May 2008.

[1] Frost boils in the Arctic are a manifestation of patterned ground in the form of nonsorted circles. Active frost boils involve convection of water through the soil that can bring basic salts from depth to the surface. As such, active frost boils can mitigate acidification and thereby strongly influence the type of vegetation supported by Arctic soils. The presence or absence of active frost boils is thought to play a pivotal role in establishing the sharp demarcation between moist nonacidic tundra (MNT) and moist acidic tundra (MAT) in the Arctic. The focus of this paper is to corroborate the predictions of a mathematical model that relates observable patterned ground features to ecosystem parameters with observations at the field sites along the North American Arctic Transect (NAAT) established by the Biocomplexity of Patterned-Ground Ecosystems Project. Model predictions indicate that recurrent one-dimensional frost heave can become unstable and evolve into multidimensional differential frost heave (DFH). A laboratory frost heave simulation produced a 28-cm pattern in an active layer of 10 cm, which agrees with linear stability theory predictions. A finite element solution predicts three-dimensional patterns with approximately 3-m spacing develop in a 1.0-m active layer with a surface *n* factor of 0.35, which agrees well with field observations from the NAAT. The lack of significant frost boil activity in the MAT is a result of suppression of DFH owing to denser surface vegetation characterized by low *n* factors. Prominent active frost boils are observed in the MNT at higher latitudes with more sparse vegetation characterized by higher *n* factors that promote DFH. However, at the northernmost field sites frost boils cannot be generated even though the *n* factors are relatively high owing to very rapid freezing conditions that mitigate DFH.

Citation: Peterson, R. A., and W. B. Krantz (2008), Differential frost heave model for patterned ground formation: Corroboration with observations along a North American arctic transect, *J. Geophys. Res.*, *113*, G03S04, doi:10.1029/2007JG000559.

1. Introduction

[2] Many cold climate regions subject to recurrent freezing and thawing can display prominent patterned landforms such as hummocks, frost boils, and stone circles. These are examples of patterned ground, i.e., surface features made prominent by the segregation of stones, ordered variations in ground cover, or regular topography [*Krantz*, 1990]. One of the patterned ground features observed in arctic tundra ecosystems is frost boils: nonsorted circles that are characterized by the absence of vegetation in the center with areas of vegetation and peat in between, as shown in Figure 1. Horizontally nonuniform (differential) frost heave (DFH) occurs within the soils of these patterns, with circle centers heaving somewhat more than the intercircle regions, although the differential heave can vary from slight to dramatic [*Nicolsky et al.*, 2008]. The characteristic size and spacing of these patterns can vary by geographic location where variations in both climate and vegetation combine to influence the thermal and hydraulic regime of the active layer and underlying permafrost. Although some pattern characteristics such as thaw depth can evolve over time, the pattern spacing (i.e., number density) in a particular area is relatively fixed on a timescale of 1000 years or more [*Hallet and Prestrud*, 1986]. The striking regularity of these patterns suggests that some characteristics of the local ecosystem, such as climate and surface vegetation, must have dictated the particular spacing when the pattern first developed. A corollary is that a measurement of the current pattern spacing could provide information about the past ecosystem when the pattern first developed.

[3] Nonsorted circles in the form of frost boils are of particular interest with respect to the role that they play in influencing vegetation. It is well known that Arctic soils gradually acidify owing to the influence of aerobic bacteria in breaking down water-soluble salts present in these soils. However, since active frost boils involve cellular convection

[1]Department of Mechanical Engineering, University of Alaska Fairbanks, Fairbanks, Alaska, USA.
[2]Department of Chemical and Biomolecular Engineering, National University of Singapore, Republic of Singapore.

0148-0227/08/2007JG000559$09.00

Figure 1. Frost boils, a form of nonsorted circle, on Howe Island, Alaska, in summer. Barren centers of mineral soil are 1–2 m across and only slightly domed. Intercircle regions are vegetated with peat. Photograph by A. Kade.

similar to earth hummocks [see *Mackay*, 1980], water containing basic salts permeates from depth to the surface thereby mitigating the effect of acidification [*Bockheim et al.*, 1998]. Indeed, the sharp demarcation line between moist nonacidic tundra (MNT) and moist acidic tundra (MAT) manifest by markedly different plant communities is thought to be due to significant frost boil activity in the former but not in the latter [*Walker et al.*, 1998]. This observation provoked this study that employs a fully predictive mathematical model to relate the observable properties of patterned ground to ecosystem variables, in particular vegetation cover quantified in terms of the *n* factor.

[4] *Washburn* [1956] identified 19 mechanisms that could influence the formation of patterned ground in recurrently frozen soils. Of those, predictive models based on first principles have been advanced for the frost-cracking [*Lachenbruch*, 1961], Rayleigh free convection [*Ray et al.*, 1983], and buoyancy-induced soil circulation [*Hallet and Waddington*, 1992] mechanisms. It is doubtful whether these aforementioned mechanisms can explain the occurrence of nonsorted circles such as frost boils in arctic tundra (Figure 1). Frost cracking is only apparent in some areas, and does not occur on the same spatial scale as that of nonsorted circles. The small density differences developed during soil freezing or thawing have been shown to be insufficient to promote buoyancy-induced free convection in most soils [*Hallet and Waddington*, 1992].

[5] More recently, attention has been directed to DFH as a possible mechanism for some types of patterned ground formation. *Kessler et al.* [2001] included DFH as an important mechanism in their predictive model for sorted stone circle formation, but relied on empirical parameterization for the DFH length scale that unfortunately has no obvious physical basis. The model also requires sorting of stones from mineral soil, and therefore cannot explain the genesis of nonsorted circles such as frost boils. The first fully predictive model for patterned ground formation via the DFH mechanism was advanced by *Peterson and Krantz* [2003]. They carried out a linear stability theory (LST) analysis that predicted the conditions (e.g., soil permeability, unfrozen moisture content, overburden pressure) required for one-dimensional frost heave to spontaneously evolve into multidimensional DFH. Their analysis also predicted the characteristic spacing of the patterns, which is a function of the soil thermal conditions during freezeup. However, the model is incomplete. Since the analysis was based on LST, it necessarily can describe only the inception of DFH rather than the evolution of more developed patterned ground forms. Furthermore, their use of a constant temperature or heat transfer coefficient at the soil surface is inadequate for describing the more complicated thermal conditions of tundra vegetation with probable snow cover

during freezeup. *Fowler* [2003] has also shown that spatial instabilities can occur in one-dimensional frost heave with a constant ground surface temperature, and given a parametric criterion for occurrence in terms of dimensionless parameters. It appears that this criterion corresponds with the physical conditions initially described by *Peterson and Krantz* [2003] and explained further here, however, no physical explanation of the instability criterion was given. *Fowler* [2003] does not address the effects of ground surface insulation due to vegetation and snow.

[6] Because of these earlier model predictions, a study was initiated to determine the role that DFH plays in the formation, stability, and transformation (e.g., alkalization) of nonsorted patterned ground features along a North American Arctic Transect (NAAT) as part of a larger "Biocomplexity of Patterned-Ground Ecosystems" project [see *Walker et al.*, 2008]. The existing DFH model using LST had two deficiencies that precluded its immediate use in describing the nonsorted circles along the NAAT. First, the energy balance at the ground surface had to be generalized to include a description that can account for the widely varying effects of surface vegetation. Second, the model had to be expanded beyond the realm of LST where the differential frost heave is assumed to be infinitesimally small. These limitations are addressed in this paper.

[7] First we briefly review the development of the LST model of *Peterson and Krantz* [2003], and then use it to demonstrate that DFH can spontaneously initiate in arctic tundra soils that undergo recurrent freezing and thawing. The complicated effects of vegetation on the soil thermal regime are described using the n factor, an empirically determined parameter recently used to describe the surface energy balance of some arctic tundra systems [*Klene et al.*, 2001] including sites along the NAAT [*Kade et al.*, 2006]. We then present the first nonlinear stability theory analysis for the DFH mechanism that permits predicting the longer term evolution of pattern development. We use this nonlinear model to determine the final pattern spacing that can develop in arctic tundra soils, and demonstrate how the vegetation quantified in terms of the n factor affects the final pattern. The strengths and limitations of LST in describing DFH initiation are discussed.

[8] Some emphasis in this paper will be on the underlying physics of DFH and on its implications for patterned ground formation. The mathematical details of the LST analysis are straightforward but tedious and are available from *Peterson and Krantz* [2003]. Only the principal equations that describe the significant processes affecting DFH are discussed in detail. The mechanism and necessary conditions for spontaneous initiation of DFH will be clearly identified. The role that surface vegetation plays in determining the pattern spacing (i.e., number density) that will evolve is discussed, and comparisons with field data along the NAAT are made. In addition, a pilot experiment to spontaneously generate patterns via DFH in the laboratory is discussed.

[9] It is important at the outset to emphasize the difference between mature patterned ground features, and small patterned perturbations in an otherwise homogeneous medium. The spontaneous initiation of the latter and the effect that vegetation has on the patterns that develop are the foci of this paper. Mature patterned ground features, particularly those with living surface vegetation, clearly owe the state of their current equilibrium condition also to spring and summer-related processes when plant growth, pooling, thaw-induced surface motion (e.g., solifluction), and nonuniform thaw occur. The initiation model we present depends on ecosystem parameters when the pattern first developed, which are likely different that the current state. Thaw depths have evolved and soil horizons have developed synergistically with frost boils. Therefore, it is not possible to use characteristics of the current system in an initiation model. Turning this around, however, points to perhaps the model's greatest utility. The pattern characteristics the model predicts such as pattern size and spacing can provide some information about ecosystem variables such as thaw depth and vegetation when the pattern first developed. Therefore, the model will be presented first, followed by comparison with laboratory and field observations. Finally, more general implications for vegetation in patterned ground systems are discussed.

2. Methods

2.1. Physics and Model Description

[10] Differential frost heave (DFH) refers to laterally nonuniform uplifting of the ground surface due to freezing of water within the soil. Frost heave can greatly exceed that due merely to the expansion of water upon freezing ($\sim$9%) owing to additional water being drawn upward via cryostatic suction [*Vignes-Adler*, 1977; *Gilpin*, 1979]. This arises because soils are wet preferentially by unfrozen water rather than ice [*Engemann et al.*, 2004]. Hence, the ice within a pore is separated from the soil by a thin film of unfrozen water. Owing to different nearest neighbor molecular interactions (e.g., London dispersion forces) in this thin film of unfrozen water, the pressure parallel to the pore wall will be less than the normal component [*Wettlaufer et al.*, 1996]. This anisotropic pressure phenomenon, often referred to as "disjoining pressure," in combination with curvature effects causes a depression in the normal freezing point T_0 that is described by

$$\frac{T_0 - T}{T_0} = \frac{(p_i - p_w)}{\rho \Delta H_f} \tag{1}$$

where $\rho = \rho_w \cong \rho_i$ is the mass density of liquid water, which is approximately the same as for ice, and ΔH_f is its latent heat of fusion. The difference between the ice pressure p_i and the unfrozen water pressure (parallel to the pore wall) p_w is proportional to the unfrozen water content and hence to the temperature. The latter relationship varies markedly between different soil types [*Andersland and Ladanyi*, 2004] and is referred to as the "soil characteristic function." This implies that the pressure gradient in the thin film of unfrozen water will be parallel to the temperature gradient, thereby providing a driving force (i.e., cryostatic suction) for upward water permeation during freezing.

[11] Frost heave is characterized by two competing processes both of which are functions of the unfrozen water content within the frozen fringe. The first process involves the disjoining pressure, which increases as the thickness, d, of the thin layer between the ice and soil particles becomes thinner. It is the gradient in this pressure resulting from the temperature gradient that causes regelation [*Gilpin*, 1979].

Theoretical descriptions of the intermolecular forces (e.g., van der Waals forces) predict that this force is proportional to d^{-3} [*Wettlaufer and Worster*, 2006]. In the model of Fowler and Krantz used here, the net force per area is described by the characteristic curve

$$p_i - p_w = \frac{(1-S)^p}{S^q} \tag{2}$$

where S is the unfrozen volume fraction of the pore space ($0 \leq S \leq 1$), and the exponents p and q are empirical constants that describe a particular soil [*Fowler and Krantz*, 1994]. The unfrozen water content is clearly related to the unfrozen water film thickness and exists because of both premelting and curvature effects. The exponents in equation (2) are experimentally determined for natural soils because the highly irregular particle shapes, orientations, and moderate size distributions make theoretical calculation a formidable task. At high unfrozen volume fractions that approach 1, p is the dominant parameter that describes how the disjoining pressure behaves as the unfrozen water content changes. The second important process is the flow of liquid water toward the growing ice lens, which can be described by Darcy's law with a hydraulic conductivity that is a function of S

$$k_h = k_0 S^{\gamma} \tag{3}$$

where k_0 is the hydraulic conductivity of the soil when no ice is present in the pore space, and γ is an experimentally determined parameter [*Fowler and Krantz*, 1994]. Both the disjoining pressure and the hydraulic conductivity are functions of S, which in turn is a function of the total pressure at the freezing front. The total force acting downward at the lowest ice lens is the summation of the overburden of the frozen soil above it, and any extra load pressure such as buildings or roads. In naturally occurring patterned ground, the extra load pressure is zero. When DFH occurs, there is more ice accumulation underneath the peaks, which has the effective result of increasing the overburden locally (i.e., the thickness of the frozen region increases).

[12] Since soils have a pore size distribution, ice penetration will progress from the larger to the smaller pores as the temperature decreases. Hence, freezing in a water-saturated soil will not occur at a discrete plane, but rather within a relatively thin (0.1–1 cm) region that is referred to as the "frozen fringe." When a sufficient amount of ice is present in the pores of the soil, it can support the entire overburden load and thereby form an ice lens. This ice lens will thicken as the frost penetration progresses further into the soil. It ceases to thicken when the ice content in the soil below the lowest ice lens becomes sufficiently high to suppress the permeation of liquid water to the ice lens. The process then repeats itself, thereby forming a series of discrete ice lenses whose thickness increases owing to the decrease in the rate of frost penetration. As a result of drawing up unfrozen water from depth to form these ice lenses, the ground surface heave can vastly exceed that due to the 9% volume expansion of liquid water upon freezing.

[13] The unsteady mass balance for water and ice, and energy balance within a freezing, saturated soil of constant porosity are [*O'Neill and Miller*, 1985; *Fowler and Krantz*, 1994]

$$\frac{\partial S}{\partial t} + \nabla \cdot \mathbf{U} = -\frac{m}{\rho} \tag{4}$$

$$\frac{\partial (1-S)}{\partial t} + \nabla \cdot \mathbf{V} = \frac{m}{\rho} \tag{5}$$

$$-Lm + \rho C_p \frac{dT}{dt} = k \nabla^2 T \tag{6}$$

where $\mathbf{U}$ and $\mathbf{V}$ are the water and ice velocity, m is mass freezing rate, C_p is heat capacity, L is latent heat of fusion, and k is thermal conductivity. The sensible heat and latent heat of a freezing soil are removed through the soil surface when the air temperature drops below freezing. The soil surface temperature is determined using an energy balance that must account for air temperature, insulation, wind, snow, topography, soil properties, soil moisture and vegetation [*Klene et al.*, 2001]. *Peterson and Krantz* [2003] previously used an overall heat transfer coefficient that has no direct correspondence with the net effect of all these processes. A new parameterization technique is used here to that can be directly related to the thermal conditions in vegetated, snow covered tundra.

[14] During active layer freezeup of an arctic tundra soil in autumn, snow depths can be relatively shallow and greatly influenced by the type of vegetation that tends to prevent snow from being blown away by the wind. The n factor has been used to parameterize the complex overall energy balance, and is defined as

$$n = \frac{\int (T_S - T_f) dt}{\int (T_a - T_f) dt} \tag{7}$$

where T_S is the soil surface temperature, T_a is the air temperature, and T_f is the normal freezing point of water. The time integral is often performed over an entire season, and average daily temperatures are used in a discrete integral (summation). An n factor near 1.0 indicates little effect of insulation because the air and soil temperatures are similar. Values significantly less than 1.0 indicate greater insulation (with a minimum value of zero due to the second law of thermodynamics). Values greater than 1.0 are possible when radiation plays a significant role in the energy balance, but are not typical for tundra systems during autumn freezeup. *Kade et al.* [2006] measured soil surface temperatures inside and outside patterned ground features at many sites along the NAAT, and calculated both summer and winter n factors, defined by whether the daily mean soil surface temperature (T_S) was above or below 0°C, respectively. It is the winter n factors that are relevant when frost heave occurs.

2.2. Model Domain and Boundary Conditions

[15] Figure 2 shows a cross section of a water-saturated soil undergoing freezing downward from the ground surface at z_s. Snow cover and vegetation occupy the region $z > z_s$.

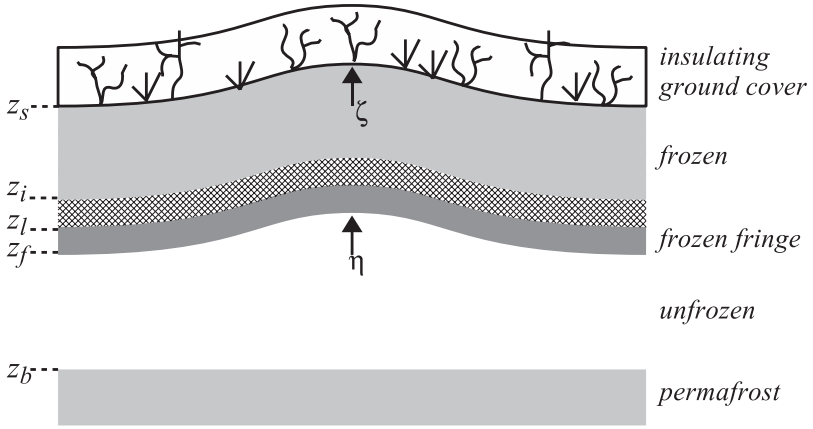

Figure 2. Schematic cross section of a water-saturated soil undergoing freezing downward from the ground surface at z_s; z_b is the permafrost table; the active layer region between z_s and z_b undergoes seasonal freezing and thawing; the frozen fringe is bounded by z_f, the plane defining the maximum instantaneous freezing depth, and z_l, the plane at which active ice lens growth occurs; between z_l and z_i, additional pore water is freezing although no additional ice lens formation or growth occur; the region between z_i and z_s undergoes no additional phase change; the planes defined by z_f, z_l, and z_i move downward, whereas that defined by z_s moves upward in time. Perturbation amplitudes in z_s and z_f from the one-dimensional solution are shown by ζ and η, respectively. Figure is not to scale.

Here we show z_b as a fixed plane defining the permafrost table that is assumed to be at 0°C, in which case the region between z_s and z_b undergoes seasonal freezing and thawing. Note that the DFH mechanism does not require that permafrost be present. However, the presence of permafrost can facilitate patterned ground formation since it helps to keep the unfrozen soil water-saturated by hindering drainage. It is well established that the permafrost table is not planar once surface features have developed, but becomes bowl shaped [*Kokelj et al.*, 2007]. However, the nonplanar shape is a consequence of positive feedback with the established surface pattern, and does not play a role in pattern initiation. The frozen fringe is bounded by z_f, the plane at 0°C that defines the maximum instantaneous depth at which freezing of pore water is occurring, and z_l, the plane at which active ice lens growth occurs. Between z_l and z_i, additional pore water is freezing although no additional ice lens formation or growth occur since the lowermost ice lens blocks any upward water permeation to this region. The region between z_i and z_s, containing ice lenses and pore ice, undergoes essentially no additional freezing. The planes defined by z_f, z_l, and z_i move downward whereas that defined by z_s moves upward in time.

[16] The Miller model involves solving the one-dimensional form of equations (4), (5), and (6) in each of the regions described above, although *Fowler and Krantz* [1994] have demonstrated using dimensional scaling that some terms can be neglected in different regions. The original Miller model also invoked a rigid ice approximation whereby the ice velocity was assumed to be constant throughout the frozen soil. *Fowler and Krantz* [1994] recognized that this assumption does not permit DFH and incorporated a regelation mechanism suggested by *Gilpin* [1979] for which the ice velocity is proportional to the local temperature gradient. This results in a set of five coupled partial differential equations in two dependent variables, the temperature and unfrozen water pressure, in two independent variables, time and the vertical spatial coordinate. The initial conditions correspond to unfrozen water-saturated soil at 0°C. The boundary conditions are continuity of temperature at 0°C, heat flux, and pressure at z_f, continuity of the temperature according to equation (1), and a load pressure equal to the weight of the overlying frozen soil and ice lenses at z_l.

[17] One major modification to previous modeling efforts that we make is important for accurately describing frost heave in vegetated soils. Whereas *O'Neill and Miller* [1985] considered only a constant subfreezing temperature boundary condition at z_s, here we consider an overlying conducting layer of snow and vegetation, with continuity of temperature at the interface but differing thermal conductivities. While other thermal boundary conditions are possible (such as constant temperature or constant heat flux), snow covered vegetation is the most common condition observed in areas of nonsorted circles in arctic tundra.

[18] Several investigators [e.g., *Black and Miller*, 1985; *Black*, 1995] have solved the Miller model for one-dimensional freezing and heave. The model as outlined above is cumbersome, subject to numerical convergence problems owing to the frozen fringe, and not readily extended to multidimensional (differential) frost heave. *Fowler* [1989] applied scaling analysis to the Miller model and showed that quasi-steady state conditions apply within all three regions and that the frozen fringe can be collapsed to a plane across which jump boundary conditions apply. Moreover, he demonstrated that a permeation boundary layer existed below the lowest ice lens across which the entire pressure drop in the water phase essentially occurs. *Fowler and Noon* [1993] have shown that the solution to this simplified model, which can be solved analytically, gives results in excellent agreement with a numerical solution to the full Miller model. *Krantz and Adams* [1996] proved that this simplified model agrees well with one-dimensional frost heave measurements in laboratory core experiments. Subse-

quently, *Fowler and Krantz* [1994] generalized the equations for the simplified Miller model to multidimensional frost heave. However, they made no attempt either to solve these multidimensional equations or to explore their implications for DFH and patterned ground formation.

[19] *Rempel et al.* [2004] reexamined the basic principles of the Miller model and demonstrated that the liquid water pressure profile within the frozen fringe can be evaluated using an integral force balance over the entire fringe; thus removing a tenuous assumption in the model concerning the local ice pressure. *Rempel* [2007] solved the one-dimensional form of this model for step freezing using a coordinate transformation. His results are qualitatively similar to the Miller model (e.g., thicker, more widely spaced lenses with increasing depth), and quantitatively indicate less overall heave under otherwise identical conditions (A. Rempel, personal communication, 2006).

2.3. Linear Stability Theory

[20] A LST analysis seeks to determine whether a particular solution for a physical process, referred to as the "basic state," is stable with respect to infinitesimal perturbations; i.e., will it evolve to a solution that describes an alternate lower energy state of the system if any of the dependent variables are minutely perturbed. Here we seek to determine whether one-dimensional freezing and heave will spontaneously evolve into multidimensional differential frost heave. The LST model developed by Peterson and Krantz employs the basic state solution for one-dimensional freezing and heave advanced by *O'Neill and Miller* [1985], which will be briefly reviewed here.

[21] Here we will provide an overview of the LST model for DFH using a basic state given by the solution for one-dimensional frost heave of *Fowler and Krantz* [1994] for the simplified model of *O'Neill and Miller* [1985]. This involves allowing spatial perturbations in all the dependent variables appearing in the multidimensional frost heave equations; these constitute the temperature, ice and unfrozen water pressures, unfrozen water volume fraction, water permeation velocity, and the moving planes defined by z_f and z_s. The solution for any dependent variable $X'(x, y, z, t)$ is of the general form

$$X' = \hat{X}(z,t)e^{i(\alpha x+\beta y)} \tag{8}$$

where α and β are the wave numbers in the x and y (i.e., lateral) directions, respectively, for which only the real part of $\hat{X}$ has physical significance. If the basic state is either time-independent or quasi-steady state (i.e., slowly changing in time), $X'(z, t)$ will have an exponential time dependence with a growth coefficient (exponential argument) Γ. If any perturbation characterized by wave numbers α and β can be found for which $\Gamma > 0$, the basic state is unstable. The basic state for freezing is time-dependent but slowly varying; i.e., the planar freezing front and ground surface move very slowly in time. The LST provides the range of conditions that result in instability and therefore DFH. Furthermore, the LST results provide the initial conditions (i.e., relative perturbation amplitudes) for the nonlinear model to be developed in section 2.4. Because of the expected radial symmetry of patterns on flat surfaces, only two-dimensional modes characterized by wave number α are considered. Since hummocks, frost boils, and stone polygons are three-dimensional patterns, their geometrical characteristics can be related to α via Squire's transformation [*Squire*, 1933], which permits obtaining the results for three-dimensional patterns from those for two-dimensional patterns.

[22] An additional consideration for DFH is the resistance to bending offered by the frozen soil. Peterson and Krantz considered two models for this resistance: a linear purely elastic (Hookian) bending described by thin plate and shell theory [*Brush and Almroth*, 1975] and, a purely viscous resistance model suggested by *Fowler and Noon* [1993]. Laboratory experiments [*Tystovich*, 1975] indicate that frozen soil behaves elastically on short timescales. Moreover, measurements are available for the elastic modulus for frozen soils [*Andersland and Ladanyi*, 2004], whereas only estimates are available for the effective viscosity. Hence, we discuss results here only for the elastic model. Furthermore, we explore a wider range of elastic moduli (0–200 MPa) than has been previously.

2.4. Nonlinear Numerical Analysis

[23] The nonlinear model was solved using the finite element method (FEM) with quadrilateral elements. The quasi-steady state energy equation was solved in the frozen region $z_s \geq z \geq z_f$ using the Fowler and Krantz frost heave equations to describe the moving boundary at z_f. Initial perturbations to the ground surface and freezing front boundaries were sinusoidal (in accordance with LST), and the initial relative amplitude between the two boundaries was provided by the results from the LST analysis. An initial top surface amplitude of 1 mm was found to be sufficiently small to correspond with the LST results.

[24] The simulation was started at an initial freezing depth of 10 cm. Since there is a singularity in the frost heave equations when freezing begins at zero depth, a finite initial value must be used for numerical reasons. We have chosen to use 10 cm, which is characteristic of the freezing depth when diurnal fluctuations no longer strongly influence the temperature gradient at the upper boundary of the frozen fringe. At very shallow freezing depths, significant frost heave does not occur and the solution approaches that of the classic Stefan problem, which is not unstable. Also, it will be demonstrated that the higher frequency perturbations that are favored at shallow freezing depths are quickly damped and therefore not significant when freezeup is complete.

[25] The active layer in the tundra systems overlying permafrost along the NAAT ranges from about 30–90 cm [*Walker et al.*, 2008]. These simulations use a maximum freezing depth of 1.0 m to cover this entire range. Upward freezing from the permafrost is not considered at this point, and the thermal gradient in the unfrozen region above permafrost is assumed negligible. The only effect of the permafrost upper boundary location is to specify when freezing ceases. It will be demonstrated in the Results how using a depth of 1.0 m is also applicable for any active layer of lesser magnitude.

3. Results

3.1. LST Predictions

[26] The LST analysis indicates that indeed one-dimensional freezing and frost heave can be unstable and thereby

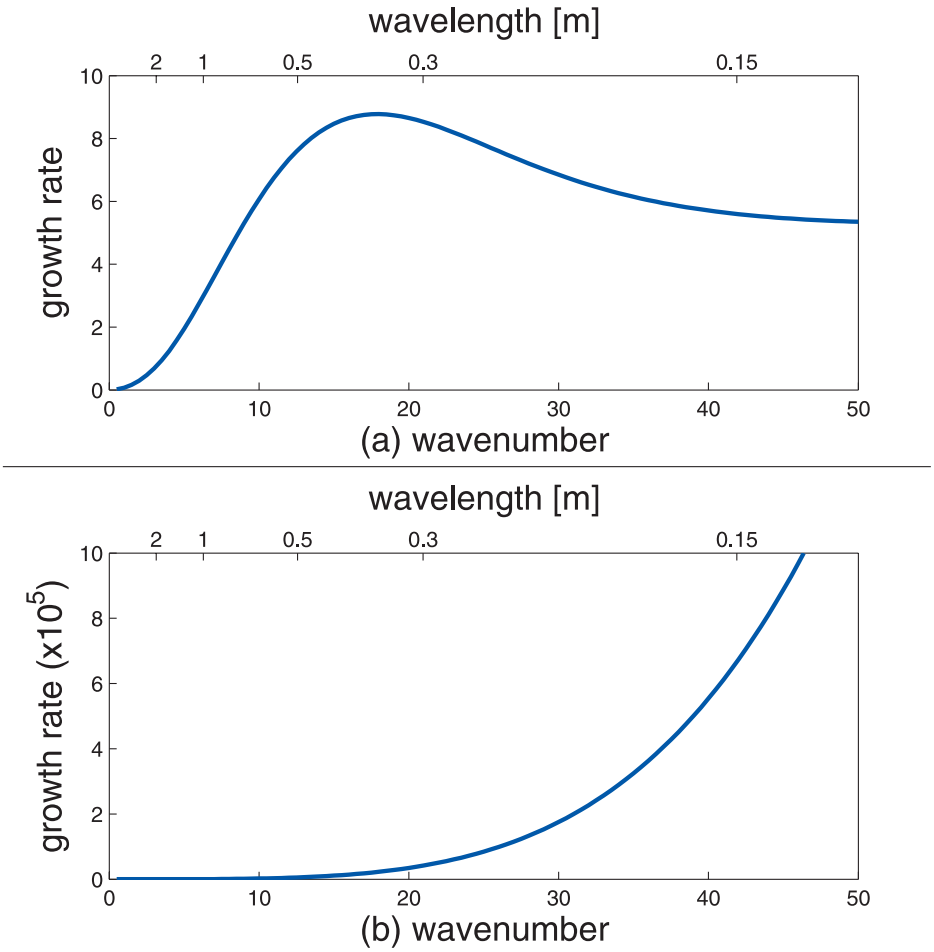

Figure 3. Results of the LST analysis showing the dimensionless growth rate as a function of dimensionless wave number for (a) zero elasticity and (b) E = 200 MPa. The corresponding dimensional wavelength is shown on the top abscissa.

display a propensity to develop into DFH. This is shown in Figure 3, which is a plot of the growth coefficient (made dimensionless with a conductive timescale) as a function of the dimensionless wave number $\alpha = 2\pi\, d_0/\lambda$, where d_0 is the maximum depth of freezing (chosen here to be 1 m, a typical active layer depth) and λ is the wavelength. The corresponding wavelength values are shown on the upper abscissa. The n factor is 0.35, which is a typical winter value in the southernmost subzone E of the NAAT, where tundra is characterized by tall tussocks, low shrubs, and thick peat [*Kade et al.*, 2006]. Larger n factors are considered later. Figure 3a corresponds to a zero-elasticity case for which the Young's Modulus E = 0. Figure 3b shows the LST results incorporating linear elasticity with E = 200 MPa. Experimental data [*Yuanlin and Carbee*, 1987] and empirical relationships [*Tystovich*, 1975; *Andersland and Ladanyi*, 2004] indicate that the modulus of frozen silt can be on the order of hundreds to thousands of MPa, with the exact value dependent on temperature and strain rate. A reasonable upper limit of the modulus for a differentially heaving soil is 2 GPa at −5°C and strain rate of 10^{-4} s^{-1}.

[27] The system is unstable under both sets of conditions. In the zero-elasticity case, there is a most highly amplified wave number of about 18 that corresponds to a wavelength of 0.35 m. When linear elasticity is included in the model, there are two significant changes in the model predictions. First, there is no longer a most highly amplified wave number in the domain of $0 < \alpha < 50$ shown here (and remains true even as $\alpha \rightarrow \infty$). Second, the magnitude of the growth rate is several orders of magnitude greater. The results in Figure 3a are similar to those of the earlier LSA of *Peterson and Krantz* [2003] where an overall heat transfer coefficient was used instead of the n factor. However, the behavior shown in Figure 3b has not been predicted heretofore. Although intuition would indicate that bending of an elastic plate might provide a resistance against DFH, the LST analysis appears to indicate that the opposite is true. The reason for this behavior is the particular trade-off between disjoining pressure and flow resistance through the frozen fringe, as explained in more detail below. Furthermore, this counterintuitive behavior only occurs when the perturbations are very small for which LST is valid. The complete nonlinear model to be developed in section 3.2 indicates that elasticity does eventually provide resistance to DFH when the perturbations are allowed to grow to finite amplitudes.

[28] Therefore, for one-dimensional frost heave to be unstable, the increase in overburden that results when extra

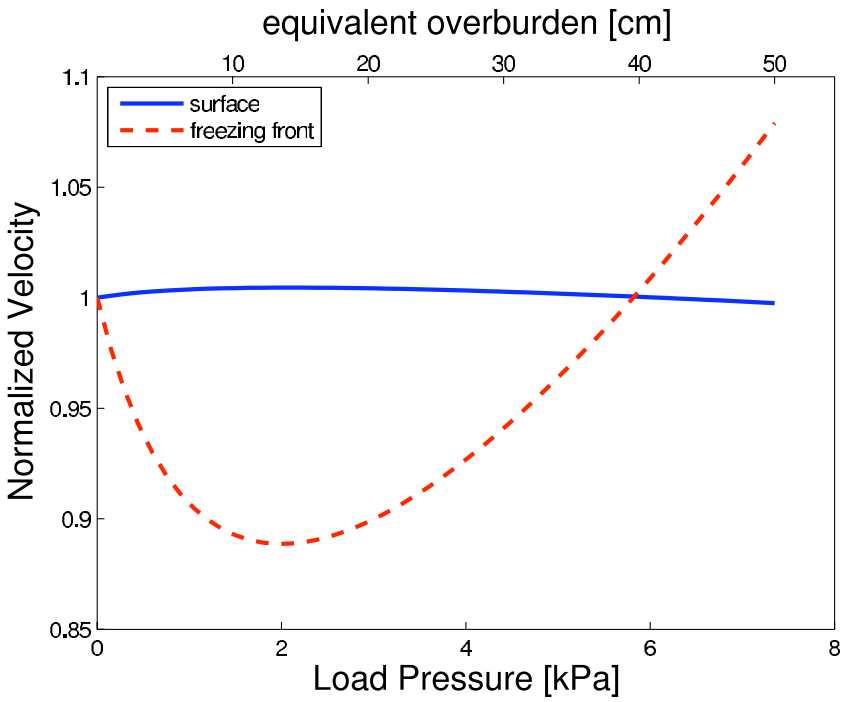

Figure 4. The upward velocity of the ground surface (solid) and the downward freezing front (dashed) velocity as a function of external load pressure. Both velocities are normalized by their zero-load value. Small increases in load pressure (<100 Pa) lead to increased surface velocity and decreased freezing-front velocity, which indicates a positive feedback mechanism during DFH. This effect disappears at load pressures above ~100 Pa.

ice accumulates must have a positive feedback that causes yet more ice to accumulate. This is in fact what happens as can be inferred from Figure 4. Here the one-dimensional ground surface and freezing front velocities are plotted as a function of the load pressure for the conditions in Figure 3a. The velocity values are normalized by their zero-load value in order to show them on the same set of axes; their exact values are not relevant to the immediate discussion. The ground surface velocity increases with load until about 2 kPa, at which point it begins to decrease. Conversely, the freezing front velocity decreases with load until about 2 kPa, at which point it begins to increase. An equivalent increase in overburden thickness is shown on the upper abscissa based on assuming a frozen soil density of 1500 kg/m^3. It is the initial slope of these curves that corresponds to the realm of LST where the perturbations are infinitesimally small. An increase in surface velocity coupled with a decrease in freezing front velocity results in a thicker overburden when the former is greater in magnitude than the latter. The LST analysis predicts that indeed $\eta/\zeta < 1$, where η and ζ are the maximum amplitudes of the freezing and ground surface fronts, thus implying that a thicker overburden does result, which has a positive feedback to further increase the overburden thickness initially. This type of instability does not occur in the classic Stefan solidification problem where the rate of freezing is also proportional to the temperature gradient. When frost heave is unstable, the increased heat flux that results when the freezing front location is perturbed results in additional heave instead of accelerated freezing at the interface. In contrast, for the classic Stefan problem the interface velocity would increase and act to damp out any perturbations. This can be verified by reducing the frost heave problem to the Stefan problem by setting the velocity term of either equation (4) or (5) equal to zero.

[29] There is yet another factor that must be considered in the case of DFH. The extra ice accumulation not only increases the overburden loading, but it changes the heat conduction path length. The isotherms are compressed in the trough relative to the crest regions. This is a consequence of the amplitude η of the perturbed freezing front at z_f always being less than the amplitude ζ of the perturbed ground surface at z_s. This implies that significant lateral temperature gradients exist to conduct heat from the crest to the trough regions, which then conduct this heat upward to the ambient air. This is confirmed by an energy balance over one wavelength, which indicates that additional frost heave occurs in the crest regions because the latent heat of fusion is conducted laterally into and upward within the trough regions. Although there is additional ice under the crest region, the increased heat flux removes the associated extra latent heat.

[30] Manifestation of this instability leading to DFH depends critically on the soil properties and instantaneous depth of freezing. After the freezing depth exceeds a critical value, positive perturbations in the overburden thickness no longer result in increasing surface velocities. A condition for instability can be determined in terms of the parameter p in equation (2), γ in equation (3), and the instantaneous depth of freezing, $z_S - z_f$. A DFH-susceptible soil must have the characteristics such that an infinitesimally small decrement in S causes an increase in disjoining pressure that is

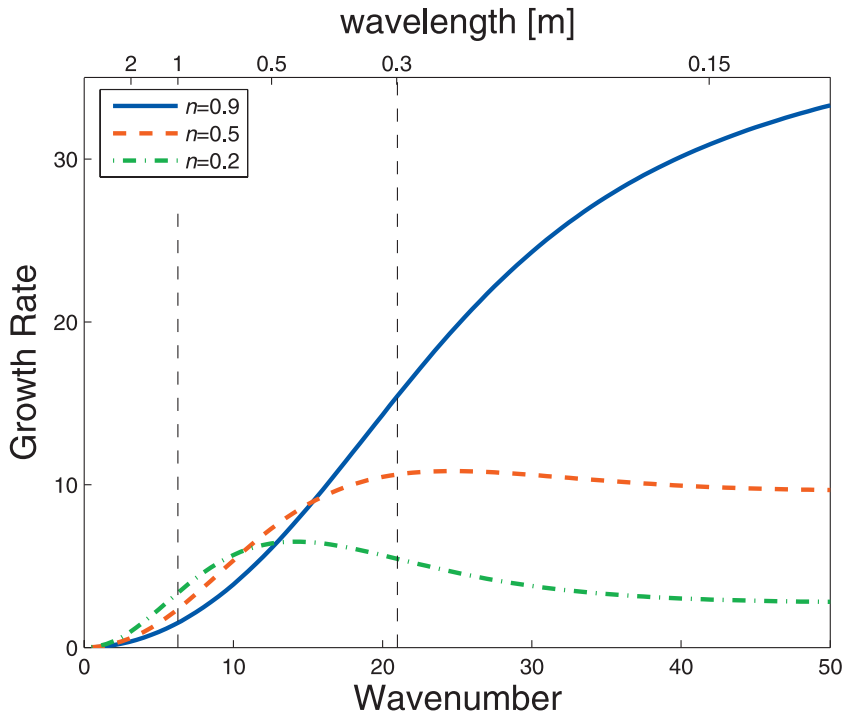

Figure 5. Results of the LST analysis for three different n factor values and an instantaneous freezing depth of 10 cm. The largest dimensionless growth rates occur with thinner snow cover and therefore less vegetation. The corresponding dimensional wavelength is shown on the top abscissa.

greater than the increase in viscous flow resistance. This condition is more readily satisfied when the overburden loading is small, and therefore is more likely to occur at shallow depths of freezing. It is important to note that it is the instantaneous depth of freezing at DFH initiation that is involved in this stability criterion rather than the total active layer thickness (i.e., maximum depth of freezing). Therefore, DFH can occur in soils with any active layer thickness and also in the absence of permafrost.

[31] The insulating effects of surface vegetation and peat are evident through changes in the n factor. Figure 5 shows the initial growth rate of perturbations for three different n factor values and the zero-elasticity case. There are two important points that should be made about these model predictions. First, the relative growth rates for these three n factors have opposite trends at small and large wave numbers. At small wave numbers less than about 10, the growth rate is greater for small n factors. At larger values of the wave number greater than about 15, the trend reverses and large n factors have larger growth rates. Therefore, for a specified wave number (or pattern size as shown on the top axis), ground surface insulation appears to either promote or mitigate DFH. The two vertical dashed lines at wavelengths of 1.0 and 0.3 indicate patterns with this opposite trend, and are discussed in more detail later.

[32] However, the size of a spontaneously generated pattern is not fixed, but corresponds to the wave number that grows most rapidly out of a continuous spectrum of possibilities. This leads to the second significant trend seen in these model predictions. For n = 0.9, there is no maximum value of the growth rate, which indicates that the fastest growing pattern is the smallest. However, for smaller n factor values beginning with about 0.5, there is a maximum growth rate value. For example, when n = 0.2, a wave number of 14 (wavelength of about 0.45 m) has the largest growth rate. When a maximum in the growth rate of a LST prediction exists, there is reason to believe that this would correspond with the final pattern that evolves since it initially grows the fastest and therefore has a head start, so to speak. However, when there is not a maximum such as for n = 0.9, it is impossible to predict the likely size of the pattern that will develop without solving the complete nonlinear model. There is also the complicating factor that the LSA results such as shown in Figure 5 are valid only for a particular instantaneous depth of freezing when the pattern first initiates. The quantitative value for growth rate and wave number vary somewhat as the instantaneous depth of freezing is varied [*Peterson and Krantz*, 2003]. A complete solution to time-dependent, nonlinear problem was sought to address this limitation and to look further into the longer-term evolution behavior of different wavelength patterns.

3.2. Nonlinear Numerical Results

[33] The LST results indicate two significant trends that necessitate corroboration by solution of the complete nonlinear model. First, a finite, most highly amplified wave number occurs for the zero elasticity case. However, the incorporation of linear elasticity results in much larger growth rates, that increase monotonically with increasing wave number. This result appears counter intuitive because the force required to bend an elastic plate should provide a stabilizing mechanism that reduces the propensity for DFH at high wave numbers. Figure 4 indicates that indeed this is true, but only at finite amplitudes that are beyond the realm of LST. Second, vegetation that decreases the n factor

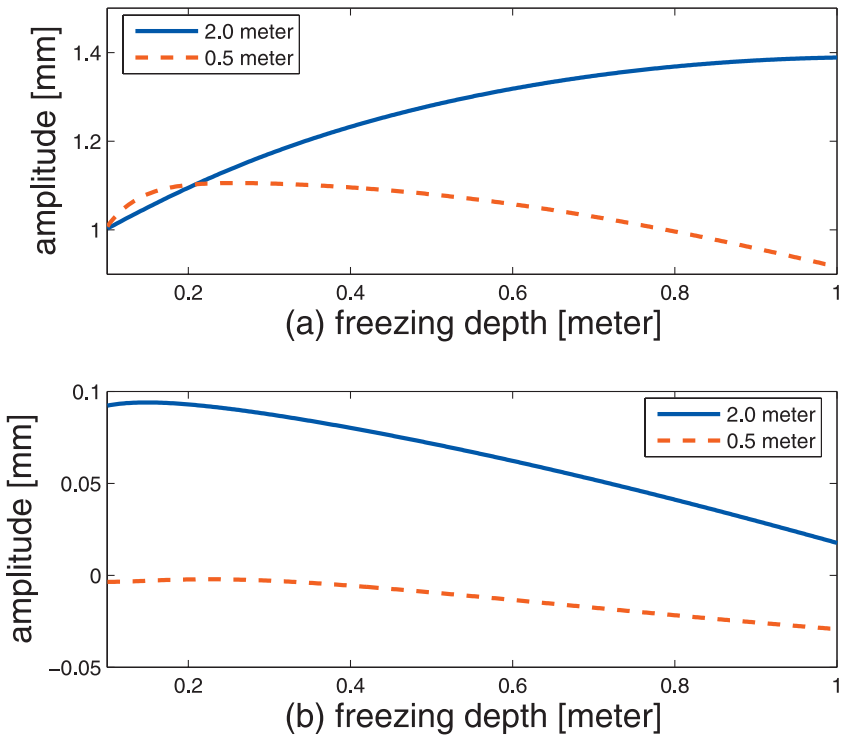

Figure 6. Evolution of the (a) ground surface and (b) freezing front perturbation amplitudes as a function of freezing depth for two different wavelengths: 0.5 m (dashed) and 2.0 m (solid). The initial amplitude ratio is specified by LST. The smaller, 0.5-m pattern initially grows faster, but the rate eventually declines as the longer, 2.0-m pattern continues to grow until completion at a freezing depth of 1.0 m.

appears to have a different effect at small and large wave numbers, which suggests there could be a correlation between pattern size and surface vegetation. Therefore a nonlinear solution to the model is required.

[34] Figure 6 shows the perturbation amplitude of both the ground surface and freezing front as a function of freezing depth for an n factor of 0.35. A wavelength of 0.5 m is shown with the dashed line, and a 2.0-m wavelength is shown with the solid line. The elastic modulus was 50 MPa for these simulations; LST predicts that shorter wavelength perturbations initially grow faster than those having a longer wavelength. Figure 6 corroborates this prediction: the amplitude initially increases faster with increasing freezing depth for the dashed relative to the solid line in Figure 6a. However, the growth rate of the 0.5-m pattern quickly begins to decrease, and at a freezing depth of about 20 cm, actually begins to decline. At the final freezing depth of 1.0 m, the amplitude of the 2.0-m pattern is over 100% larger than that of the smaller pattern. The 2.0-m pattern will eventually also decline in amplitude at even larger active layer depths, but at that point a larger pattern (e.g., 3 m) would still be increasing. This longer-term evolution through freezing of the entire active layer could not have been determined using LST, which provides only growth information at a temporary, fixed value of the freezing depth. Furthermore, the nonexponential rate of growth (or decay) of these patterns indicates that nonlinear terms have become relevant; therefore, the amplitudes cannot be obtained from an integral of the LSA-predicted exponential growth rates.

[35] The perturbation amplitude of the freezing front is shown in Figure 6b for both wavelengths. Recall that LST determines the relative amplitude of the initial perturbations (i.e., η/ζ), and that this ratio is a function of wave number. Because the initial top surface amplitude was 1 mm, the initial freezing front amplitude is adjusted to the value determined using LST. The 0.5-m pattern initially has a negative amplitude ratio according to LST. Although it is difficult to discern at this scale, the freezing front perturbations initially grow in amplitude during the first few time steps precisely as LST predicts. In fact, matching the initial growth rates of perturbations in both boundaries is how 1.0 mm was determined to be sufficiently small to match LST. Although the freezing front perturbation of the 2.0-m pattern decreases in amplitude in the long-term (from 0.09 to about 0.02 mm), the continued increase in surface relief (ground surface perturbations) indicates that DFH will continue beyond infinitesimally small perturbations, and therefore can lead to patterned ground.

[36] While LST is capable of determining the conditions under which DFH is unstable, it does appear not to provide much insight into the relative long-term behavior of different sized patterns. Recall the LST results in Figure 5 that show opposite trends at 1.0-m and 0.3-m wavelengths, as shown with the dashed lines. The growth of these two patterns during freezeup is shown in Figure 7 for three different values of the n factor. The overall trend for both pattern sizes remains the same: larger n factor values lead to more overall perturbation growth. Although LST predicts an

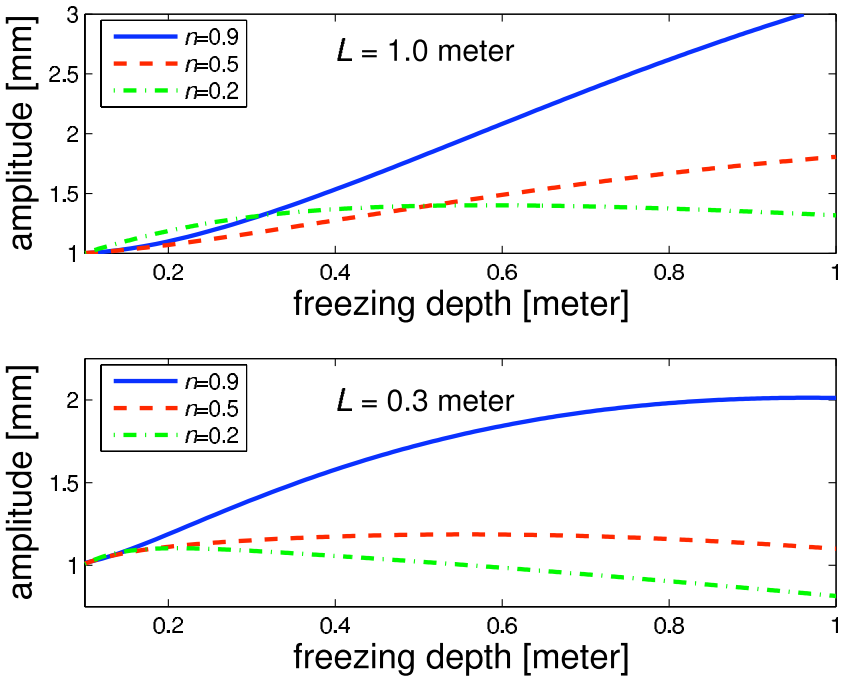

Figure 7. Evolution of the ground surface perturbation amplitude for pattern wavelengths of (a) 1.0 m and (b) 0.3 m. More net growth occurs for the larger pattern, and the trend of more growth for larger *n* factors is the same for both wavelengths, which is not evident from the LST results.

opposite trend for small wave numbers (large patterns), that initial behavior is not maintained in the longer term.

[37] The two-dimensional nonlinear results, such as shown in Figure 6, indicate that the evolution of DFH throughout freezing of the entire active layer may indeed include mode selection of a preferred wavelength. Although LST indicates that the one-dimensional system is unstable, the two-dimensional simulations indicate that nonlinear effects eventually become significant enough to change the growth rates of various wavelengths. Therefore, a significantly more computationally intensive three-dimensional simulation was performed using an initial superposition of random, two-dimensional surface perturbations. The *n* factor is 0.35 for this simulation. A contour plot of the initial ground surface is shown in Figure 8a. Figure 8a was generated by a superposition of 25 hexagonal patterns [*Christopherson*, 1940] of random wavelength, spatial offset, and submillimeter amplitude (pseudowhite noise) and still shows some slight regularity that would diminish with a greater number of patterns in the superposition. Figure 8b is a contour plot of the ground surface topography after three freeze cycles to a depth of 1.0 m. Because different modes grow at different rates as shown in Figure 6, the contour of the ground surface evolves away from the initial, random conditions. Higher-frequency modes become damped, favoring those of a longer wavelength. *Kessler et al.* [2001] observed a similar trend in their model for sorted stone circles where the dominant wavelength increased with the number of freeze-thaw cycles.

[38] Figures 8c and 8d are for six and nine freeze cycles. Mode selection of a characteristic wavelength is evident as the pattern matures. The final surface topography at the end of freezing is used as the initial topography for the subsequent cycle. This assumption overpredicts the magnitude of the surface topography by neglecting the accumulated ice volume that melts, and may be improved by using some fraction of the final amplitude based on the relative rates of vertical to horizontal soil movement during thaw. However, this assumption only affects the number of freeze cycles required for pattern stabilization, and not the final size of the pattern. The spatial scale of each frame is $4\pi \approx 12.5$ m; hence, pattern evolution appears to approach a wavelength of ~3 m, which is very similar to the interpattern spacing observed in many arctic tundra ecosystems, such as shown in Figure 1. The number of actual freeze and thaw cycles required to attain this pattern will be more, and scales with the relative rates of vertical and horizontal soil movement during thaw. The model of *Kessler et al.* [2001] predicted 1000 cycles before pattern stabilization in sorted stone circles, which corresponds with roughly about a 1% rate of horizontal to vertical soil motion. A significant improvement would be to incorporate a more complete model of thaw and solifluction, which involves the complicating factors of both elastic and plastic deformation of supersaturated soils [*Harris et al.*, 2003].

4. Discussion

4.1. Laboratory Corroboration

[39] A demanding test of any model is to validate its predictions via controlled laboratory studies. We are not aware of any prior successful attempts to grow patterned ground associated with DFH in the laboratory; moreover, only limited field experiments for pattern initiation under semicontrolled conditions have been successful [e.g., *Ballantyne*, 1996]. Key considerations were choosing a soil that readily promotes frost heave (i.e., frost suscep-

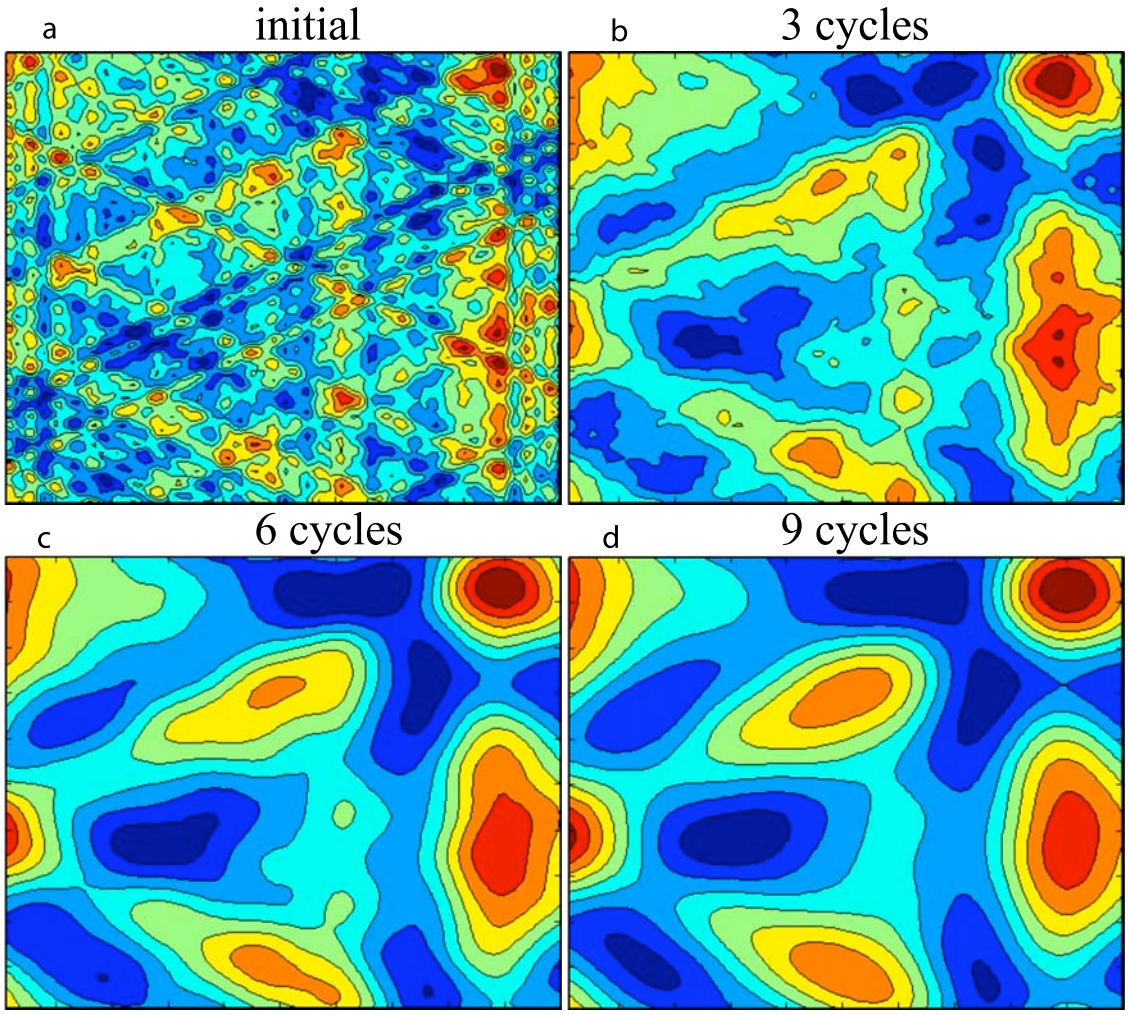

Figure 8. Contour plot of (a) the ground surface elevation initially and (b–d) at three-cycle intervals. The initial contours are pseudo-white noise with a maximum elevation of 1.0 mm. After three freezing cycles, a distinct pattern is taking shape, and the pattern appears to stabilize after nine freeze cycles. The data shown in each frame are normalized by the maximum elevation; the eight contour lines are equally spaced.

tible); assuring one-dimensional freezing and thawing; maintaining a water supply below the freezing front to sustain ice lens growth; and freezing sufficiently slowly to permit measurable frost heave. Although frost heave can occur in a closed system without an external water supply via redistribution of pore water, less overall heave results and would slow the pattern formation process. A commercial open top freezer with overhead infrared panels was programmed for daily freeze/thaw cycles to permit facilitating the growth of patterned ground on a relatively short timescale (1–2 weeks). The box depth was 15 cm, and the maximum depth of freezing never exceeded 10 cm during each cycle. Figure 9 shows a photograph of four frost boils made prominent by soil surface heave and some sorting of stones. The square box was 56 cm wide; hence, the pattern center-to-center distance was about 28 cm, which corresponds to a dimensionless wave number of 25.8. Because of symmetry requirements, only integral numbers of waves should be expected; hence, this system geometry would allow for α = 12.9, 25.8, 38.7, etc. The LST results in Figure 3a indicate that α = 25.8 is the most highly amplified wave number in the allowed set for this geometry.

[40] Pattern initiation can theoretically begin at any depth of freezing, and the maximum depth of freezing does not necessarily correspond to the depth at which DFH first begins, as is assumed in the estimates just discussed. However, there is a compelling reason to believe that this might be the case for this experiment. One-dimensional frost heave under constant ground surface thermal conditions is similar to the classic Stephan solidification problem for which the freezing depth is proportional to the square root of time. Therefore, the system spends more time at larger freezing depths. It is therefore more likely that the one-dimensional system will experience perturbations leading to DFH at larger freezing depths simply because it spends more time there.

[41] While these limited laboratory results do not provide conclusive data to validate the model described here, they do provide compelling evidence that frost heave alone can

Figure 9. Photograph of four frost boils made prominent both by soil surface heave and sorting of stone. The center-to-center spacing of about 28 cm is in agreement with the model predictions of the most likely pattern to form at a 10-cm depth of freezing. The interboil region appears darker due to greater surface ice.

lead to patterned ground. The presence of permafrost in a natural setting keeps saturation levels high by preventing drainage, but also more closely resembles a closed system where initial frost heave is supported by pore water redistribution. Permafrost also often causes some upward freezing, with final freezeup occurring at a location slightly less than the maximum active layer depth. It seems reasonable to expect that the pattern that develops in this case will correlate with this intermediate depth. Further experiments with more comprehensive monitoring of temperature, freezing rate, heave and water content are currently being performed and will hopefully shed additional light on these questions.

4.2. Comparison With Field Observations

[42] The analytical and numerical results presented thus far indicate that one-dimensional frost heave can be unstable and lead to DFH with eventual pattern formation of a characteristic size. The successful laboratory experiment previously discussed provides further motivation for investigating whether DFH might be responsible for some characteristics of patterned ground, primarily the pattern shape and spacing. Here we compare the predicted trends of the DFH model with field observations. We will focus this analysis on data recently obtained from the North American Arctic Transect (NAAT) during the Biocomplexity of Patterned-Ground Ecosystems project discussed in detail elsewhere in this volume. Figure 10 shows the locations of several key sites along this transect that will be discussed. All sites have continuous permafrost. The current state of the ecosystems at these sites is highly complex due to the vast number of interrelated processes occurring; moreover, they appear to be in a state of quasi-equilibrium with the current climate, yet susceptible to changes in climate. It would be overly optimistic to believe that the general DFH model discussed here can predict the precise pattern size based on current soil and thermal conditions since decades of positive and negative feedback have changed many characteristics of the landscape both above and below ground. It is meaningful, however, to determine if the scale of the model agrees with the patterns that are observed.

[43] The most spectacular patterned ground features (PGF) in the NAAT appear at Howe Island, for which an aerial photograph is shown in Figure 11. Here there are two prominent types of patterning that occur at different spatial scales. The larger, nonsorted circles with barren centers are 1–2 m in diameter and have center-to-center distances that range from 2 to 4 m (patterned ground of type 3 in Table 1 of *Walker et al.* [2008]). The smaller, polygonal PGF are 10–30 cm in diameter and appear to have many characteristics of a cracking network (patterned ground of type 1). Their origin may be due to either desiccation [*Weinberger*, 1999] or thermal contraction [*Sletten et al.*, 2003], and is discussed elsewhere in this volume. The larger PGF do not share several characteristics of their smaller counterparts, most notable is their near-circular geometry and also possibly a hexagonal pattern. Two distinct repeat units of this regular pattern are shown with solid lines in Figure 11. The only regular interconnected geometric forms that tile a two-

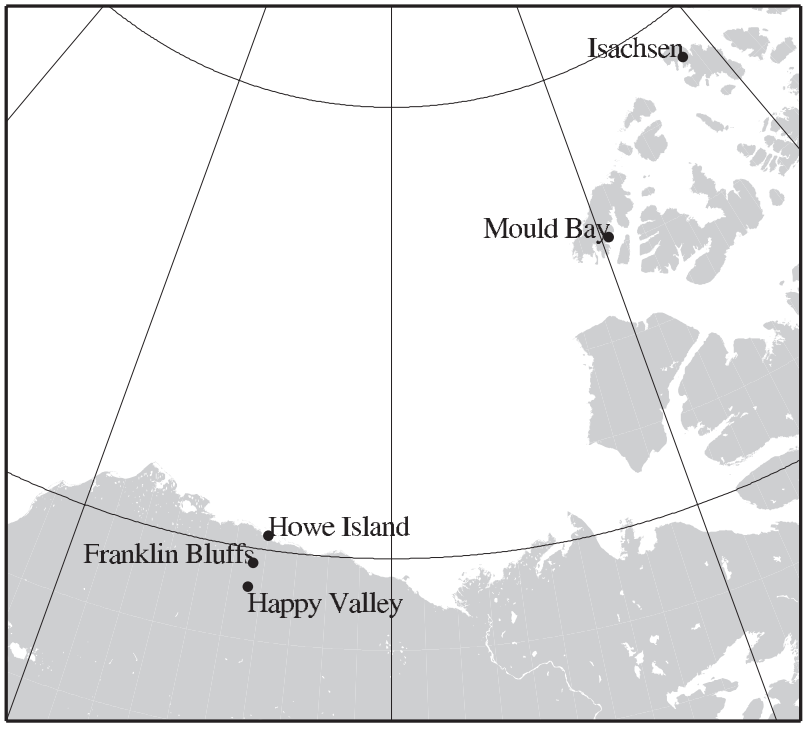

Figure 10. Five sites along a North American Arctic Transect that demonstrate a trend in type of nonsorted patterned ground. There are heavily vegetated and obscured nonsorted circles at Happy Valley, prominent nonsorted circles at Franklin Bluffs and Howe Island, and near absence at Mold Bay and Isachsen. It is possible to explain this trend with the DFH model.

dimensional plane are squares and hexagons, of which stripes and equilateral triangles are subsets, respectively. If the pattern shown in Figure 11 is formed via the model proposed here, the resulting pattern must be one of those forms. There is obviously insufficient evidence in Figure 11 to conclude that there is necessarily a hexagonal pattern and not just several circles with similar nearest neighbor distances. However, because a hexagonal pattern is one of only a very few possible according to the model proposed, it provides more supporting evidence for the model applicability to the formation of nonsorted circles.

[44] The shape and pattern of these PGF are very similar to the three-dimensional model predictions shown in Figure 8, where the features are also elliptical to circular, occur in a hexagonal pattern, and have center-to-center spacing of about 3 m. There is an obvious predisposition to forming a hexagonal pattern based on the initial conditions. This correspondence with hexagonal patterning is encouraging although not definite confirmation of the model predictions. The active layer thickness at Howe Island is approximately 80 cm beneath the feature centers and 65 cm in between, which is of the same order as the maximum freezing depth used in both the LST and nonlinear analyses. *Kade et al.* [2006] calculated the winter n factor at this site to be 0.94 at the bare circles and 0.87 in the interpattern tundra, which is close to the model predictions shown in blue on Figures 5 and 7.

[45] At inland NAAT sites slightly to the south of Howe Island such as Franklin Bluffs, the center-to-center spacing of nonsorted circles is of the same order and the active layer is also in a similar range of 65–80 cm. The winter n factor here is 0.73 on bare circles and 0.53 in the interpattern tundra [*Kade et al.*, 2006]. Further south into subzone E at Happy Valley, nonsorted circles exist but are heavily vegetated, with many patterns nearly obscured. Thicker vegetation, peat, and snow are the major cause of lower n factors at Happy Valley with values of 0.35 and 0.32 in the circles and tundra, respectively [*Kade et al.*, 2006]. The vegetation appears to mitigate frost heave; indeed, removal of the vegetation from nonsorted circles in a vegetation alteration experiment resulted in a 26% increase in heave [*Kade and Walker*, 2008]. Therefore, a more insulated ground surface (lower n factor) mitigates heave and also decreases the propensity for DFH to initiate. The modeling results discussed here support the hypothesis that the nonsorted circles at Happy Valley initially formed under less vegetated conditions. A subsequent increase in vegetation, perhaps due to climate change, has led to conditions less conducive to new pattern formation. The existing patterns remain due to positive feedback [*Shur and Ping*, 2003] but have become less prominent in the landscape.

[46] At sites north of Howe Island such as Mold Bay and Isachsen, significantly shallower active layers (25–35 cm) prevail and only the smaller, polygonal crack patterning occurs on the 10–30 cm scale. The winter n factor also declines moving north, with $n = 0.77$ at Isachsen [*Walker et al.*, 2008]. Although smaller n factors are less susceptible to spontaneous pattern formation, this alone cannot explain the absence of nonsorted circles here. One possible explanation for the near absence of nonsorted circles is the shallower active layer and corresponding shorter freezeup time, which

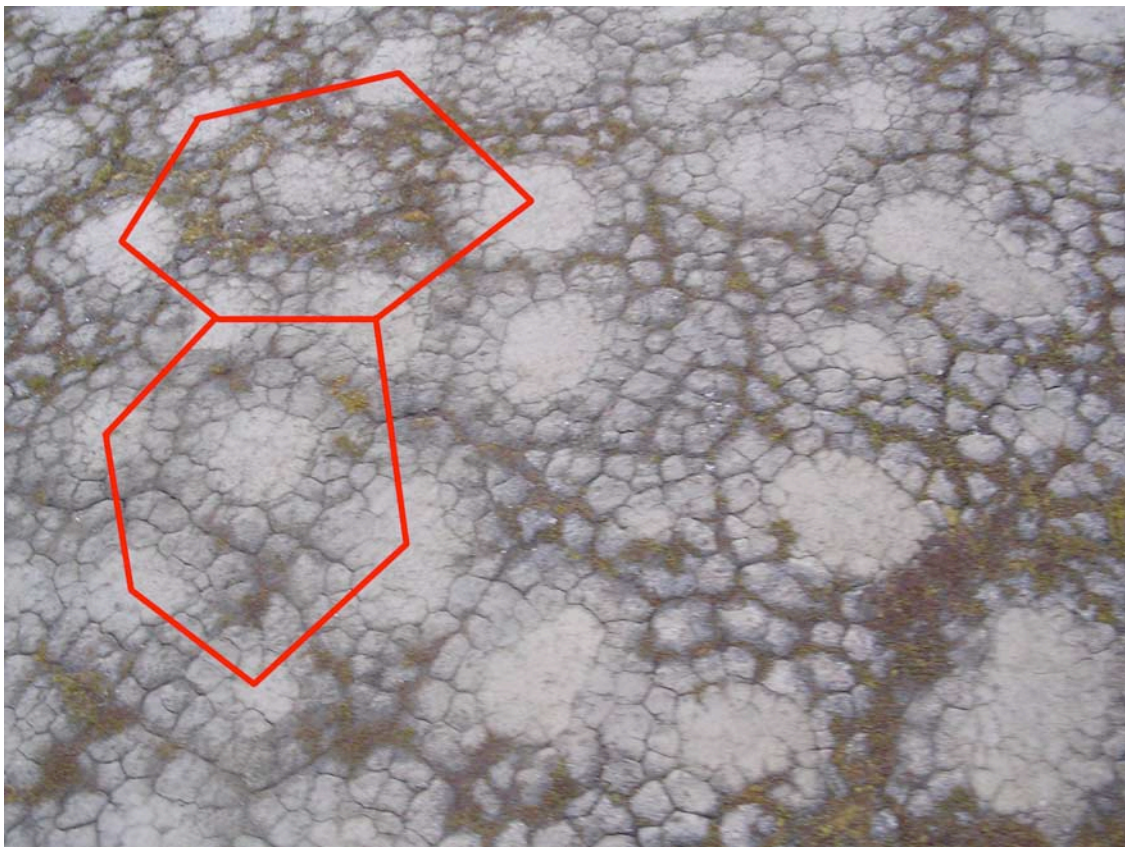

Figure 11. Aerial photograph of Howe Island showing two types of patterning on different spatial scales. Small-scale polygonal features 10–30 cm across are present in conjunction with larger, nonsorted circles 1–2 m in diameter and spaced 2–4 m apart. A hexagonal pattern that agrees with the model is possible, and two repeat units are outlined with thick lines. Photo by A. Kade.

may leave insufficient time for DFH to initiate. The mechanism for spontaneous initiation of DFH discussed here requires somewhat precise conditions where differential ice lens thickening occurs with a relatively large unfrozen volume fraction (S in equations (4) and (5)) below the growing lens. These conditions are less likely to occur at very shallow freezing depths where lenses are thin and closely spaced, and the thermal gradients are stronger. Another possible explanation is simply that the soil at more northern sites does not have the particular characteristics that make it susceptible to DFH discussed earlier; namely, a greater increase in disjoining pressure than decrease in hydraulic conductivity when the ice content increases. Unfortunately, accurate measurement of these two soil characteristics in the laboratory has proven difficult and inconclusive, and yet may still not be representative of natural conditions in the field.

4.3. Implications for Tundra Vegetation

[47] The major implication of this modeling analysis for tundra vegetation is that DFH leads to circulation of groundwater within the active layer. This provides an explanation for the sharp pH boundary between moist nonacidic tundra (MNT) and moist acidic tundra (MAT) in the Arctic foothills of Alaska discussed by *Walker et al.* [1998]. At lower Arctic latitudes dense vegetation, characterized by relatively low n factors, suppresses patterned ground formation. At mid-Arctic latitudes, higher n factors and relatively slow freezing conditions promote DFH that is manifest in particular as frost boils, a form of nonsorted circles. These frost boils bring basic salts from depth that mitigate acidification of the soil and thereby promote a markedly different plant community from that observed at lower latitudes. However, at high Arctic latitudes freezing occurs too rapidly to permit DFH and the patterned ground forms arising from it. The sharp demarcation between MNT and MAT is dramatic enough to be observed via color-enhanced remote sensing [*Walker et al.*, 1998] and is a consequence of the markedly different plant communities supported on nonacidic (pH > 5.5) versus acidic soils. Nonacidic soil conditions can be maintained if conditions permit active frost boil activity.

[48] This study also has implications for vegetation under conditions of climate change and its associated northward shift in summer temperatures and winter snowpack. In addition to the obvious direct consequences of changing temperature and snow on vegetation, the emergence of new patterned ground by DFH, or the cessation of water circulation by DFH, will affect the soil chemistry. Studies have shown that soils with nonsorted circles have lower carbon to nitrogen ratios, greater microbial activity, and more decomposed organic fractions [*Michaelson et al.*, 1996; *Walker et al.*, 2008].

[49] Finally, this analysis indicates how differences in vegetation between pattern centers and the interpattern regions can be the result of DFH and the patterns that develop. For example, surface relief leads to pooling in the interpattern regions in the summer while the pattern centers are relatively drier. However, while it is possible to conclude that DFH can lead to spatial vegetation differentiation, the reverse has not been directly demonstrated here. It would be straightforward to apply a variable *n* factor boundary condition on the ground surface and solve the heave equations in multiple dimensions. DFH will occur under these conditions, but the longer term dynamics during one or several freeze thaw cycles are a function of positive and negative feedbacks under variable surface thermal conditions (i.e., *n* factors) that are difficult to predict. This modeling approach is addressed by *Nicolsky et al.* [2008].

5. Conclusions

[50] Frost heave is a common occurrence in arctic tundra ecosystems where soil saturation levels are high because underlying permafrost prevents significant drainage of snowmelt and rain. Differential frost heave (DFH) can spontaneously occur for soils with particular characteristics of their partially frozen state where disjoining pressure and hydraulic conductivity are highly nonlinear functions of the ice content. Linear stability theory (LST) has been used to clearly identify the necessary conditions for instability when a natural soil is undergoing freezing below a vegetated snow cover. A critical positive feedback related to how small increases in overburden affect the relative rates of heave and freezing velocities is identified as a cause for instability in one-dimensional frost heave. LST predicts a finite most highly amplified wave number when the Young's modulus of the frozen soil approaches zero and *n* factors are less than 0.9, while use of higher modulus values results in growth rates that increase monotonically with wave number. This behavior is due to a limitation of LST where perturbations to the basic state are assumed to be infinitesimally small.

[51] Solution of the time-dependent frost heave model in two and three dimensions indicates that high wave number perturbations are eventually damped, and a pattern of a finite wavelength eventually results. LST also predicts that patterns larger than $\sim$1 m grow faster with small *n* factors, with an opposite trend for small patterns. The full solution of the time-dependent model shows that this is not the case, and larger *n* factors favor pattern development of all sizes. This prediction supports the theory that insulating vegetation mitigates the development of new patterned ground and that patterns in highly vegetated locations may have initially formed under less vegetated conditions.

[52] Although LST does not accurately predict the dominant pattern size that develops after one or more complete freezing events, it is still the only method to accurately determine the conditions for which one-dimensional frost heave is unstable. The spontaneous generation of a pattern from an otherwise smooth system necessarily begins with infinitesimally small perturbations when LST is accurate and valid. Therefore, we can rely on LST to predict the conditions for instability regardless of how and when the nonlinear effects of finite-sized perturbations become significant.

[53] A controlled pilot laboratory simulation of one-dimensional freezing has shown that DFH as well as sorting of small clasts can occur on a scale that is consistent with the stability theory predictions. The laboratory results demonstrate that the existence of permafrost is not a necessary condition for DFH to initiate when sufficient subterranean water is supplied. Observations of nonsorted patterned ground at some sites along a North American Arctic Transect also indicate characteristic pattern spacing consistent with the predictions of the DFH model. The prevalence of nonsorted circles at Howe Island is well supported by the model predictions but fails to adequately predict the absence of any nonsorted circles at more northern locations such as Isachsen. Although several interrelated physical, biological, and hydrological processes currently act to sustain the observed patterns, DFH is a viable mechanism for the initial pattern formation.

[54] **Acknowledgments.** We wish to acknowledge Dave Huber, Martin Linck, and Jeremy Lee for performing the laboratory experiments. This paper has benefited from discussion and data from Skip Walker and Vlad Romanovsky. Photographs were taken by Anya Kade. Helpful comments from two anonymous reviewers greatly improved the paper. Funding from NSF grant OPP-0120736 is also gratefully acknowledged.

References

Andersland, O. B., and B. Ladanyi (2004), *Frozen Ground Engineering*, 2nd ed., 363 pp., John Wiley, Hoboken, N. J.

Ballantyne, C. K. (1996), Formation of miniature sorted patterns by shallow ground freezing: a field experiment, *Permafrost Periglacial Processes*, *7*, 409–424, doi:10.1002/(SICI)1099-1530(199610)7:4<409::AID-PPP230>3.0.CO;2-3.

Black, P. B. (1995), RIGIDICE model of secondary frost heave, *CRREL Tech. Rep. 95-12*, U.S. Army Cold Reg. Res. and Eng. Lab., Hanover, N. H.

Black, P. B., and R. D. Miller (1985), *A Continuum Approach to Modeling Frost Heave*, Am. Soc. of Civ. Eng., New York.

Bockheim, J. G., D. A. Walker, L. R. Everett, F. E. Nelson, and N. I. Shiklomanov (1998), Soils and cryoturbation in moist nonacidic and acidic tundra in the Kuparuk river basin, Arctic Alaska, U.S.A., *Arct. Alp. Res.*, *30*(2), 166–174, doi:10.2307/1552131.

Brush, D. O., and B. O. Almroth (1975), *Buckling of Bars, Plates, and Shells*, pp. 80–88, McGraw-Hill, New York.

Christopherson, D. G. (1940), Note on the vibration of membranes, *Q. J. Math.*, *os-11*, 63–65, doi:10.1093/qmath/os-11.1.63.

Engemann, S., H. Reichert, H. Dosch, J. Bilgram, V. Honkimaki, and S. Snigirev (2004), Interfacial melting of ice in contact with SiO_2, *Phys. Rev. Lett.*, *92*(20), 205701, doi:10.1103/PhysRevLett.92.205701.

Fowler, A. C. (1989), Secondary frost heaving in soils, *SIAM J. Appl. Math.*, *49*, 991–1008, doi:10.1137/0149060.

Fowler, A. C. (2003), *A Mathematical Model for Differential Frost Heave, Proc. Int. Conf. Permafrost*, vol. 1, edited by M. Philips, S. M. Springman, and L. Arenson, pp. 249–252, A. A. Balkema, Lisse, Netherlands.

Fowler, A. C., and W. B. Krantz (1994), A generalized secondary frost heave model, *SIAM J. Appl. Math.*, *54*(6), 1650–1675, doi:10.1137/S0036139993252554.

Fowler, A. C., and C. G. Noon (1993), A simplified numerical solution of the Miller model of secondary frost heave, *Cold Reg. Sci. Technol.*, *21*(4), 327–336, doi:10.1016/0165-232X(93)90010-6.

Gilpin, R. R. (1979), A model of the "liquid-like" layer between ice and a substrate with applications to wire relelation and particle migration, *J. Colloid Interface Sci.*, *68*, 235–251, doi:10.1016/0021-9797(79)90277-7.

Hallet, B., and S. Prestrud (1986), Dynamics of periglacial sorted circles in western Spitsbergen, *Quat. Res.*, *26*(1), 81–99, doi:10.1016/0033-5894(86)90085-2.

Hallet, B., and E. C. Waddington (1992), Buoyancy forces induced by freeze-thaw in the active layer: implications for diapirism and soil circulation, in *Periglacial Geomorphology*, edited by J. C. Dixon and A. D. Abrahams, pp. 251–279, John Wiley, Chichester, U.K.

Harris, C., M. C. R. Davies, and B. R. Rea (2003), Gelifluction: Viscous flow or plastic creep?, *Earth Surf. Processes Landforms*, *28*(12), 1289–1301, doi:10.1002/esp.543.

Kade, A., and D. A. Walker (2008), Experimental alteration of vegetation on nonsorted circles: Effects on cryogenic activity and implications for

climate change in the Arctic, *Arct. Antarct. Alpine Res.*, *40*(1), 96–103, doi:10.1657/1523-0430(06-029)[KADE]2.0.CO;2.

Kade, A., V. E. Romanovsky, and D. A. Walker (2006), The n-factor of nonsorted circles along a climate gradient in Arctic Alaska, *Permafrost Periglacial Processes*, *17*, 279–289, doi:10.1002/ppp.563.

Kessler, M. A., A. B. Murray, B. T. Werner, and B. Hallet (2001), A model for sorted circles as self-organized patterns, *J. Geophys. Res.*, *106*(B7), 13,287–13,306, doi:10.1029/2001JB000279.

Klene, A. E., F. E. Nelson, N. I. Shiklomanov, and K. M. Hinkel (2001), The n-factor in natural landscapes: variability of air and soil-surface temperatures, Kuparuk River Basin, Alaska, USA, *Arct. Antarct. Alp. Res.*, *33*, 140–148, doi:10.2307/1552214.

Kokelj, S. V., C. R. Burn, and C. Tarnocai (2007), The structure and dynamics of earth hummocks in the Subarctic forest near Inuvik, Northwest Territories, Canada, *Arct. Antarct. Alp. Res.*, *39*, 99–109, doi:10.1657/1523-0430(2007)39[99:TSADOE]2.0.CO;2.

Krantz, W. B. (1990), Self-organization manifest as patterned ground in recurrently frozen soils, *Earth Sci. Rev.*, *29*, 117–130.

Krantz, W. B., and K. E. Adams (1996), Validation of a fully predictive model for secondary frost heave, *Arct. Alp. Res.*, *28*, 284–293, doi:10.2307/1552107.

Lachenbruch, A. J. (1961), Depth and spacing of tension cracks, *J. Geophys. Res.*, *66*, 4273–4292, doi:10.1029/JZ066i012p04273.

Mackay, J. R. (1980), The origin of hummocks, western Arctic coast, Canada, *Can. J. Earth Sci.*, *17*, 996–1006.

Michaelson, G. J., C. L. Ping, and J. M. Kimble (1996), Carbon storage and distribution in tundra soils of Arctic Alaska, USA, *Arct. Alp. Res.*, *28*(4), 414–424, doi:10.2307/1551852.

Nicolsky, D. J., V. E. Romanovsky, G. S. Tipenko, and D. A. Walker (2008), Modeling biogeophysical interactions in nonsorted circles in the low Arctic, *J. Geophys. Res.*, doi:10.1029/2007JG000565, in press.

O'Neill, K., and R. D. Miller (1985), Exploration of a rigid ice model of frost heave, *Water Resour. Res.*, *21*, 281–296, doi:10.1029/WR021i003p00281.

Peterson, R. A., and W. B. Krantz (2003), A mechanism for differential frost heave and its implications for patterned ground formation, *J. Glaciol.*, *49*, 69–80, doi:10.3189/172756503781830854.

Ray, R. J., W. B. Krantz, T. N. Caine, and R. G. Gunn (1983), A model for sorted patterned ground regularity, *J. Glaciol.*, *29*, 317–337.

Rempel, A. W. (2007), The formation of ice lenses and frost heave, *J. Geophys. Res.*, *112*, F02S21, doi:10.1029/2006JF000525.

Rempel, A. W., J. S. Wettlaufer, and M. G. Worster (2004), Premelting dynamics in a continuum model of frost heave, *J. Fluid Mech.*, *498*, 227–244, doi:10.1017/S0022112003006761.

Shur, Y., and C. L. Ping (2003), The driving force of frost boils and hummocks formation, *Eos Trans. AGU*, *84*(46), Fall Meet. Suppl., Abstract C21B-0823.

Sletten, R. S., B. Hallet, and R. C. Fletcher (2003), Resurfacing time of terrestrial surfaces by the formation and maturation of polygonal patterned ground, *J. Geophys. Res.*, *108*(E4), 8044, doi:10.1029/2002JE001914.

Squire, H. B. (1933), On the stability of three-dimensional disturbances of viscous flow between parallel walls, *Proc. R. Soc. London, Ser. A*, *142*, 621–628, doi:10.1098/rspa.1933.0193.

Tystovich, N. A. (1975), *The Mechanics of Frozen Ground*, 426 pp., McGraw-Hill, New York.

Vignes-Adler, M. (1977), On the origin of the water aspiration in a freezing dispersed medium, *J. Colloid Interface Sci.*, *60*, 162–171, doi:10.1016/0021-9797(77)90267-3.

Walker, D. A., et al. (1998), Energy and trace-gas fluxes across a soil pH boundary in the arctic, *Nature*, *394*(6692), 469–472, doi:10.1038/28839.

Walker, D. A., et al. (2008), Arctic-patterned-ground ecosystem: A synthesis of studies along a North American Arctic Transect, *J. Geophys. Res.*, doi:10.1029/2007JG000504, in press.

Washburn, A. L. (1956), Classification of patterned ground and review of suggested origins, *Geol. Soc. Am. Bull.*, *67*, 823–865, doi:10.1130/0016-7606(1956)67[823:COPGAR]2.0.CO;2.

Weinberger, R. (1999), Initiation and growth of cracks during desiccation of stratified muddy sediments, *J. Struct. Geol.*, *21*, 379–386, doi:10.1016/S0191-8141(99)00029-2.

Wettlaufer, J. S., and M. G. Worster (2006), Premelting dynamics, *Annu. Rev. Fluid Mech.*, *38*, 427–452, doi:10.1146/annurev.fluid.37.061903.175758.

Wettlaufer, J. S., M. G. Worster, L. A. Wilen, and J. G. Dash (1996), A theory of premelting dynamics for all power law forces, *Phys. Rev. Lett.*, *76*(19), 3602–3605, doi:10.1103/PhysRevLett.76.3602.

Yuanlin, Z., and D. L. Carbee (1987), Tensile strength of frozen silt, *CRREL Rep. 87-15*, U.S. Army Cold Reg. Res. and Eng. Lab., Hanover, N. H.

W. B. Krantz, Department of Chemical and Biomolecular Engineering, National University of Singapore, Republic of Singapore, 117576.

R. A. Peterson, Department of Mechanical Engineering, University of Alaska Fairbanks, Fairbanks, AK 99775, USA. (rorik@alaska.edu)